Available online at www.sciencedirect.com
SCIENCE DIRECT®
Surface Science 572 (2004) 239–246
SURFACE SCIENCE
www.elsevier.com/locate/susc

X-ray scattering study of the stoichiometric recovery of the α-$Fe_2O_3(0001)$ surface

C.-Y. Kim [a,*], A.A. Escuadro [a], M.J. Bedzyk [a], L. Liu [b], P.C. Stair [b]

[a] *Department of Materials Science and Engineering and Institute for Environmental Catalysis, 2220 Campus Drive, Northwestern University, Evanston, IL 60208, USA*
[b] *Department of Chemistry and Institute for Environmental Catalysis, Northwestern University, Evanston, IL 60208, USA*

Received 5 July 2003; accepted for publication 26 August 2004
Available online 17 September 2004

Abstract

The stoichiometric recovery and accompanying changes of subsurface atomic structure of Ar ion sputtered, oxygen deficient α-$Fe_2O_3(0001)$ are studied with X-ray scattering. Although oxygen annealing up to 735 °C results in a stoichiometric top surface layer manifested as a (1×1) surface structure, the X-ray scattering reveals the existence of a non-stoichiometric phase in the subsurface region. The non-stoichiometric region is characterized as a remnant of Fe_3O_4 or γ-Fe_2O_3. The stoichiometric outmost surface layers act as a barrier for propagation of oxidation to underneath remnant phase. The remnant phase can be removed after annealing at a higher temperature.

Keywords: Iron oxide; Oxidation; X-ray scattering, diffraction, and reflection; Surface structure, morphology, roughness, and topography; Sputtering

1. Introduction

Recent interest in metal oxide surfaces is due to applications in heterogeneous catalysis, corrosion and gas sensing [1]. Determination of the atomic structure of the clean surface provides a basis for further study of chemical reactions on the surface. The main obstacle for studies of chemical reactions on metal oxide surfaces resides in difficulties of generating a well-defined clean stoichiometric surface. To prepare clean metal oxide surfaces several cleaning methods have been used. These methods include ion sputtering followed by oxygen annealing [2], vacuum annealing [3], and oxygen annealing [4]. Since annealing can cause the segregation of bulk impurities to the surface, repeated cycles of sputtering and annealing are widely used for cleaning oxides. However, because ion sputtering favors the removal of oxygen atoms over metal atoms, non-stoichiometric surface regions can be

* Corresponding author. Tel.: +1 8474917677; fax: +1 8474672269.
E-mail address: cykim@northwestern.edu (C.-Y. Kim).

0039-6028/$ - see front matter © 2004 Elsevier B.V. All rights reserved.
doi:10.1016/j.susc.2004.08.036

induced [5,6]. In many cases recovering a stoichiometric surface after sputter-induced reduction requires annealing in an oxygen environment. Since the chemical composition of oxide surfaces has a significant effect on its chemical properties, the recovery of stoichiometry should be checked carefully. Various experimental methods have been used to quantify the chemical composition (stoichiometry) of oxide surfaces. In photoemission measurements, distinct oxidation states of cation or defect states in valence spectra have been used to measure the amount of reduction [2,6]. Often surface reconstruction found at a specific surface composition can be used as an indication of a reduced surface, which can be monitored with LEED [6]. Ion scattering has also been used to map the depth profile of chemical composition [7]. However, if the chemical composition of a reduced sample varies with the depth below the surface, it is difficult to get a complete picture of stoichiometric recovery based only on surface-sensitive measurements.

The hematite (α-Fe_2O_3)(0 0 0 1) surface has been known to produce different surface reconstructions depending on the surface preparation [8,9]. Ion sputtering will preferentially remove oxygen from the oxide surface and generate a FeO_x ($x = 1$) film [6]. Subsequent oxygen annealing of the reduced surface results in different surface structures that are dependent on the annealing temperature and oxygen partial pressure. Annealing under an oxygen partial pressure less than 1×10^{-7} Torr (including vacuum annealing) changes the FeO_x film to a thick magnetite (Fe_3O_4) layer by extracting oxygen atoms from underlying hematite [10–12]. Different surface structures form upon annealing under higher oxygen pressure [13]. One surface reconstruction is the so-called 'biphase' structure, which has been observed over a wide range of oxygen partial pressure and annealing temperature [14]. This structure can be identified by a floriated (1×1) LEED pattern. Recent STM results have shown that the biphase surface is actually composed of three different structures of the topmost Fe atomic layers [14]. The authors speculated the origin of the biphase as reduced oxygen coverage under the top iron layer. Despite intensive studies of reduced surface structures, most of the experiments are limited to a probing depth of several top atomic layers and cannot provide structural information beneath the surface layers.

In this paper, we use X-ray scattering to study the structural changes of subsurface regions caused by various oxygen annealing treatments of sputter-reduced hematite (0 0 0 1) surfaces.

2. Experimental

Surface preparation and X-ray scattering measurements were performed in an UHV chamber coupled to 2 + 2 geometry diffractometer at the NSLS X16A beamline [15]. The UHV chamber had a base pressure of 2×10^{-10} Torr and is equipped with LEED, AES, sputtering gun and gas sources. High quality natural hematite single crystal ($10 \times 10 \times 1\,mm^3$, Commercial Crystal Laboratories) was degreased before installing into UHV chamber. The X-ray fluorescence measurement from the sample showed major impurities of Ca, Mn, Na and K with total amount less than 0.5 wt%. In a separate X-ray photoelectron spectroscopy measurement, only K was detectable (less than 0.01 ML) after sputter-annealing. The sample was mounted on top of a heater consisting of a Mo housing and a tungsten filament embedded in alumina. The sample was sputter-cleaned using 500 eV Ar^+ ions for 20 min at a 1.5 μA sample current. The sputter-reduced samples were treated using several molecular and atomic oxygen annealing conditions. There were no further structural changes after 30 min annealings. Sample temperatures were measured by an optical pyrometer that uses the ratio of two different infrared wavelengths for temperature calibration. The accuracy of the measurements in absolute temperature was within ±50 °C. The error in relative temperature between each measurement was ±3 °C. For atomic oxygen annealing, the atomic oxygen was generated by flowing nitrous oxide (N_2O) gas through a hot quartz tube [16], producing mostly atomic oxygen and molecular nitrogen. The distance from the tube end to sample surface was 20 mm. Before each oxidation treatment the substrate was re-sputtered under the same condition.

Away from the Bragg points (which are sensitive to the bulk crystal structure), diffracted X-ray intensity due to the surface region is concentrated in crystal truncation rods (CTRs) which originate at the bulk peaks and are oriented perpendicular to the surface [17,18]. The so-called ridge scan was used to obtain the CTR profiles where intensities taken from a scan through backgrounds were subtracted from the peak intensities [19]. To check the validity of the ridge scan, rocking scans were performed at a few points along CTRs after different annealing treatments. Even though some of the rocking scans, especially on the low L side, show main peaks sitting on a very broad backgrounds, there was no change in broad background features as the annealing condition varies. Under this circumstance the CTR profiles obtained from a ridge scan can produce the same CTR profiles extracted from rocking scans at every points. CTRs were measured in a UHV condition after cooling the sample to RT in the same oxygen environment used during the anneal.

3. Results and discussion

To utilize the high reactivity of the atomic oxygen, an Ar ion sputtered sample was annealed with atomic oxygen generated from cracked N_2O gas. The LEED pattern was (1×1) after annealing at 525 °C in 2×10^{-6} Torr chamber pressure. The actual gas pressure at the sample surface could be higher than the chamber pressure due to the directional gas flux from the gas cracker tube. The $(0\,0\,0\,L)$ CTR profile from the surface was similar to that from the sample annealed at the 645 °C under molecular oxygen partial pressure of 1×10^{-5} Torr. The LEED pattern changed from (1×1) to $\left(2\sqrt{3}/3\times2\sqrt{3}/3\right)R30^\circ$ after increasing the annealing temperature from 525 °C to 720 °C. The $(0\,0\,0\,L)$ CTR profile after annealing at 720 °C temperature is shown in Fig. 1(a). In addition to the bulk Bragg peak at $L=6$, there are sharp diffraction peaks located at $L=2.85$ and 5.70. It has been shown that re-oxidation with an insufficient supply of oxygen converts reduced hematite to magnetite [11,12]. The hematite has the corundum structure and magnetite has the inverse spinel structure. It is worth noting that the γ-Fe_2O_3 with the spinel structure can be formed after a low temperature oxidation of magnetite [20]. With a high temperature anneal, there are two possible crystallographic orientation relations between magnetite and the underlying hematite substrate [21]. Along the surface normal direction, the magnetite $\langle1\,1\,1\rangle$ direction is aligned with the surface normal $\langle0\,0\,0\,1\rangle$ direction of the hematite substrate. For in-plane directions, either the magnetite $\langle1\,1\,\bar{2}\rangle$ (A) or 60° rotated $\langle\bar{1}\,2\,\bar{1}\rangle$ (A′) directions are aligned with the $\langle1\,0\,0\,0\rangle$ direction of the substrate. Fig. 1(b) shows Bragg peaks from two possible azimuthal orientations of magnetite along the CTR of the hematite substrate. Note the broad feature under the sharp magnetite peaks along the specular rod, especially around $L=2.95$. Previous

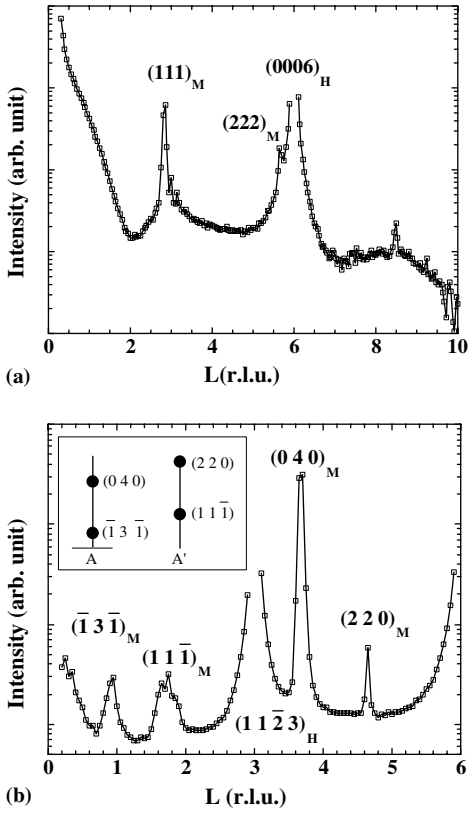

Fig. 1. (a) $(0\,0\,0\,L)$ and (b) CTR from atomic oxygen annealed sample. Inset in (b) note the Bragg peaks from magnetite with two possible azimuthal orientation relations with hematite substrate.

XANES measurements reported that annealing of sputtered hematite at 1×10^{-6} Torr O_2 at 700 °C for 30 min produced a magnetite film while annealing for 90 min at the same conditions turned the whole subsurface region to hematite [10]. However, as evidenced by X-ray scattering it was not possible to remove the magnetite phase under the annealing conditions used in this study of 30 min annealing at 2×10^{-5} Torr oxygen partial pressure and 745 °C sample temperature. The magnetite phase showed no significant changes even after 10 h of annealing at the same condition. The significance of the kinetics in this oxidation process needs further study. Remaining experiments were performed with a new substrate and the molecular oxygen annealing methods were used.

As shown in Fig. 2, the sharp Bragg peaks from the magnetite phase were absent in specular rods after molecular oxygen annealing. However, the broad features around the positions where Bragg peaks from the magnetite phase seen on the atomic oxygen annealed sample persist until annealing at 745 °C in 2×10^{-5} Torr of molecular oxygen partial pressure. The effect of Ar ion sputtering on the broad feature centered at $L = 2.95$ r.l.u. was examined by comparing the $(0\,0\,0\,L)$ specular rod before and after sputtering (not shown). Although the broad feature around $L = 2.95$ disappeared after sputtering, the thickness fringe around $L = 1.0$ remained nearly unchanged. The thickness fringe can be understood as the change from a phase causing broad features to a disordered $Fe_{1-x}O$ phase upon sputtering.

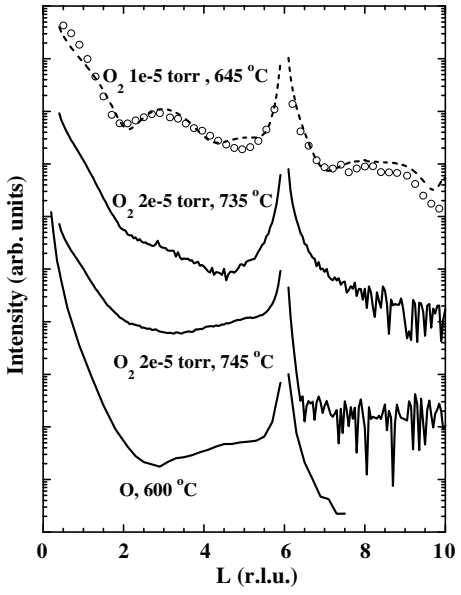

Fig. 2. The $(0\,0\,0\,L)$ CTR profiles for different annealing treatments. Dashed line represents the intensity fit on the basis of the '1–2–3' model.

Based on the peak positions in the specular rod and the effect of sputtering, the origin of the broad feature can be assigned to small domains of poorly ordered magnetite phase. This remnant phase can be considered as an indication of an incomplete conversion of magnetite to hematite. From the width of the broad peak at $L = 2.95$ the thickness of the remnant phase was estimated as 10 ± 1 Å based on the Sherrer equation assuming the remnant phase to be a uniform layer. The two-dimensional unit cells formed by oxygen anions have dimensions of 2.97 Å for the magnetite (1 1 1) surface and 2.90 Å for the hematite (0 0 0 1) surface [22]. The magnetite unit cell should be reduced by 2.4% and rotated 30° to match the underlying (1×1) hematite unit. The center of the broad peak at $L = 2.95$ corresponds to 3.5% expansion of the lattice constant along the surface normal direction from the unstrained magnetite phase, which would have a peak at $L = 2.85$. Considering the interlayer distance of 4.84 Å between the magnetite (1 1 1) planes, the thickness of the remnant phase matches with two repeating units of strained magnetite along the $\langle 1\,1\,1 \rangle$ direction (10.02 Å) within experimental error. However, X-ray scattering from the broad features could not be used to distinguish poorly ordered magnetite from γ-Fe_2O_3 due to their similar structures and lattice constants.

As seen in Fig. 2, the intensities of the broad features diminished with increasing annealing temperature. Although X-ray scattering indicates the existence of remnant magnetite, a (1×1) LEED phase was produced after annealing with 2×10^{-5} Torr oxygen pressure up to 735 °C. Hendewerk et al. [23] have reported similar results from water adsorption–annealing treatment where it was observed that the outermost surface layers of reduced hematite were re-oxidized while a reduced species remains below the surface. After molecular

oxygen annealing at a sample temperature of 745 °C, the $(0\,0\,0\,L)$ rod profile changed dramatically. Our LEED measurement showed that the surface structure has changed to biphase. The biphase was successfully converted to (1×1) upon atomic oxygen annealing at 625 °C while the $(0\,0\,0\,L)$ rod profile was similar to that from the biphase.

Fig. 3 shows the oxygen annealing effect on the $(0\,1\,\bar{1}\,L)$ crystal truncation rod. The remnant phase is manifested as broad peaks around $L = 3$ and 5. The broad peak at $L = 3$ is closely related to a peak from magnetite at $L = 2.85$ along the $(0\,0\,0\,L)$ specular rod. A poor in-plane order of the remnant phase with a relatively well-defined interlayer distance could cause a broad intensity distribution at the surface normal momentum transfer corresponding to that interlayer distance. The broad feature in rod can be interpreted as a result of the interference between the substrate hematite CTR and the broad intensity distribution of poorly ordered magnetite or γ-Fe_2O_3 remnant. Similarly the peak at $L = 5.0$ can be related to the peak $L = 5.7$ along $(0\,0\,0\,L)$ rod, corresponding to the (2 2 2) Bragg peak of a remnant phase. The existence of a broad feature around $L = 5$ along the specular direction can be seen clearly in Fig. 4 of the rod profile from a surface sputtered for only 10 min. In this case, the shorter sputtering process was unable to remove the entire magnetite phase. The appearance of broad feature around $L = 5$ in the partially sputtered sample implies that the origin of the broad feature extends deep into the subsurface region. The broad features around $L = 3$ and 5 were not observed from the well-developed magnetite phase of the first sample annealed in atomic oxygen.

For further atomic structural analysis, a simple '1–2–3' model has been applied to fit $(0\,0\,0\,L)$ CTR from the substrate with the remnant phase. The model is based on a single Fe layer terminated hematite (0 0 0 1) surface. To mimic the remnant phase, the Fe atoms in octahedral sites in the sixth and seventh layers of hematite have been replaced with three layers of the Fe atoms either in tetragonal or in octahedral sites. The (0 0 0 1) CTR taken from the substrate annealed at 645 °C under a molecular oxygen partial pressure of 1×10^{-5} Torr was fitted with program ROD [24]. The CTR profile obtained from the fitting is shown as the dashed line in Fig. 2. The relaxations obtained from the $(0\,0\,0\,L)$ rod fit were used to simulate the $(0\,1\,\bar{1}\,L)$ rod. In simulations the Fe atoms in remnant layers were assumed to have high symmetry in-plane positions with equal spacing along

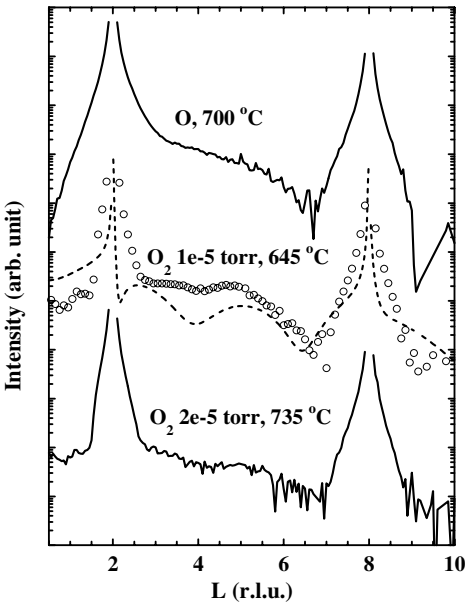

Fig. 3. The $(0\,1\,\bar{1}\,L)$ CTR taken from different stages of recovery process. Dashed line corresponds to the calculated intensity according to the '1–2–3' model with layer relaxations obtained from the $(0\,0\,0\,L)$ CTR fit.

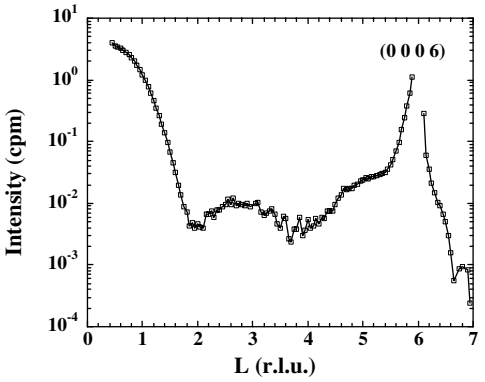

Fig. 4. $(0\,0\,0\,L)$ CTR taken from partially sputtered substrate showing clear feature around $L = 3$ and 5.

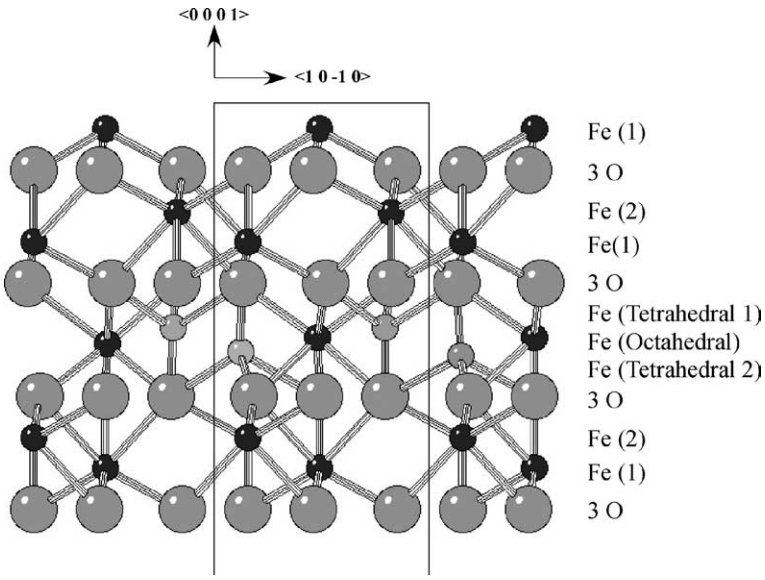

Fig. 5. Schematic side view of '1–2–3' model of the α-Fe_2O_3(0 0 0 1) surface. Large sphere corresponds to the oxygen atoms. Small dark and gray spheres represent Fe atoms in octahedral and tetrahedral sites, respectively. The unit cell is drawn in solid lines.

$\langle 1\,0\,\bar{1}\,0\rangle$ direction. With a configuration of two Fe atoms in tetragonal sites and one Fe atom in an octahedral site (Fig. 5), calculated rod profile qualitatively matches the main broad features of $(0\,1\,\bar{1}\,L)$ rod as shown in Fig. 3. Among various combinations, tetrahedral sites with in-plane coordinates of (0, 1/3) and (1/3, 1/3) and an octahedral site of (2/3, 1/3) represented as a fraction of the hematite surface unit cell gives the best CTR simulation as show in Fig. 3. It is worthwhile to note that the two tetragonal and one octahedral configuration is a common build block in magnetite and γ-Fe_2O_3 structures.

In Table 1 the interlayer distances obtained from (0 0 0 L) CTR fitting are compared with interlayer distances in bulk magnetite for remnant layers and bulk hematite for the others. Less than 30% deviation of the interlayer distances from bulk structures is comparable to results from studies of other oxide surfaces [9,25]. Despite a wide depth distribution of the remnant phase that is evident in the CTR from the partially sputtered substrate, the '1–2–3' model explains main features of remnant phase qualitatively. However, the limited data set was not sufficient to derive a definitive structure through fitting. Considering the complexity of the system and a possible contribution from minor phases often encountered in mineral samples, more complete sets of CTR profiles obtained from individual rocking scans would be necessary to characterize the remnant phase.

Table 1
Surface relaxations for α-Fe_2O_3(0 0 0 1) with remnant phase in '1–2–3' model

Layer	Interlayer distance (Å)	Bulk interlayer distance (Å)	Deviation from bulk interlayer distance (%)
Fe(1)	0.76 (17)	0.84	−10
3O	0.62 (15)	0.84	−26
Fe(2)	0.74 (12)	0.60	23
Fe(1)	0.75 (14)	0.84	−11
3O	0.72 (15)	0.63[a]	15
Fe(Tetragonal 1)	0.56 (12)	0.61[a]	−8
Fe(Octahedral)	0.62 (12)	0.61[a]	2
Fe(Tetragonal 2)	0.67 (14)	0.63[a]	6
3O	0.65 (14)	0.84	−23
Fe(2)	0.60 (12)	0.60	0
Fe(1)	0.84 (14)	0.84	0
3O			

The layers are labeled according to Fig. 5.
[a] Bulk interlayer distances from magnetite.

It is well known that low oxygen pressure ($<1 \times 10^{-7}$ Torr) annealing of sputter-cleaned hematite samples produces a magnetite film over a wide range of annealing temperatures. The X-ray scattering results indicate that while annealing at higher oxygen pressure can recover the stoichiometric hematite surface, high temperature annealing for an adequate amount of time (30 min in our study) is required to completely recover the reduced subsurface regions that have been reduced by sputtering. Annealing at higher temperatures and at high oxygen partial pressures will gradually change the remnant phase back to hematite. The biphase reconstruction is a final stage toward complete stoichiometric recovery. To our knowledge, there has been no prior atomic scale study of the oxidation process from magnetite to hematite.

Based on LEED and X-ray scattering measurements, we can postulate the stoichiometric recovery process. After low temperature annealing at a high oxygen pressure, the top surface layers are recovered to hematite. The presence of hematite at the topmost surface layers limits further oxidation of the deep layer remnant magnetite located beneath the recovered surface hematite. From the study of oxidation of iron metal, it has been known that the existence of Fe^{3+} on the top surface limits oxide growth [26]. Also, theoretical calculations predict a high-energy cost for the generation of oxygen vacancies in the subsurface oxygen layer of the hematite (0001) surface [27]. By increasing the annealing temperature, oxidation can propagate to deeper layers. While the high temperature annealing can effectively recover subsurface magnetite, the topmost surface then becomes a non-stoichiometric biphase. It has been suggested that the lattice defects (the magnetite phase can be considered as a defect to hematite) can segregate to the surface during oxidation of magnetite to hematite. The biphase can then be interpreted as a phase of oxygen defects that has segregated to the top surface region. A higher oxygen partial pressure ($>2 \times 10^{-5}$ Torr) or active atomic oxygen is necessary to convert the topmost surface layer to hematite after a high temperature annealing treatment. Although the recovery process at an even higher oxygen partial pressure was not studied in this work, we expect a similar process with different temperature dependence.

4. Conclusion

The atomic structure changes during the stoichiometric recovery process of the ion-sputtered oxygen deficient hematite (0001) surface were studied with X-ray scattering. The formation of a magnetite thin film was observed after atomic oxygen annealing. Molecular oxygen annealing at 2×10^{-5} Torr oxygen partial pressure recovered the topmost surface to a stoichiometric phase after annealing up to 735 °C. Although the surface was converted to a stoichiometric phase, a remnant phase of magnetite (or γ-Fe_2O_3) in the subsurface region was observed by X-ray scattering measurement. Increasing the annealing temperature to 745 °C removed the remnant phase and changed the topmost surface to a non-stoichiometric biphase. Atomic oxygen annealing treatment recovered the topmost surface from a biphase to a stoichiometric (1×1) phase.

Acknowledgments

This work was supported by NSF under contract No. CHE-9810378 and DOE under contract No. DE-FG02-03ER15457 to the Institute for Environmental Catalysis at NU. This research was carried out at the National Synchrotron Light Source, Brookhaven National Laboratory, which is supported by the U.S. Department of Energy, Division of Materials Sciences under contract No. DE-AC02-76CH00016.

References

[1] P.A. Cox, The Transition Metal Oxides, Oxford University Press, Oxford, 1992.
[2] D.S. Toledano, E.R. Dufresne, V.E. Henrich, J. Vac. Sci. Technol. A 16 (1998) 1050.
[3] Q. Guo, P.J. Moller, Surf. Sci. 340 (1995) L999.
[4] P. Liu, T. Kendelewicz, G.E. Brown Jr., E.J. Nelson, S.A. Chamber, Surf. Sci. 417 (1998) 53.
[5] R. Holm, S. Storp, Appl. Phys. 12 (1977) 101.

[6] R.L. Kurtz, V.V. Henrich, Surf. Sci. 129 (1983) 345.
[7] J. Ahn, J.W. Rabalais, Surf. Sci. 388 (1997) 121.
[8] R.J. Lad, V.E. Henrich, Surf. Sci. 193 (1988) 81.
[9] G. Ketteler, W. Weiss, W. Ranke, Surf. Rev. Lett. 8 (2001) 661.
[10] M. Pollak, M. Gautier, N. Thromat, S. Gota, W.C. Mackrodt, V.R. Saunders, Nucl. Instrum. Meth. Phys. Res. B 97 (1995) 383.
[11] W. Weiss, A. Barbieri, M.A. Van Hove, G.A. Somorjai, Phys. Rev. Lett. 71 (1993) 1848.
[12] A. Barbieri, W. Weiss, M.A. Van Hove, G.A. Somorjai, Surf. Sci. 302 (1994) 259.
[13] Sh.K. Shaikhutdinov, W. Weiss, Surf. Sci. 432 (1999) L627.
[14] N.G. Condon, F.M. Leibsle, A.R. Lennie, P.W. Murray, D.J. Vaughan, G. Thornton, Phys. Rev. Lett. 75 (1995) 1961.
[15] M.-T. Tang, K.W. Evans-Lutterodt, M.L. Green, D. Brasen, K. Krisch, L. Manchanda, G.S. Higashi, T. Boone, Appl. Phys. Lett. 64 (1994) 748.
[16] X.-D. Peng, R. Viswanathan, G.H. Smudde Jr., P.C. Stair, Rev. Sci. Instrum. 63 (1992) 3930.
[17] I.K. Robinson, Phys. Rev. B 33 (1986) 3830.
[18] G. Renaud, Surf. Sci. Rep. 32 (1998) 1.
[19] E. Vlieg, J. Appl. Cryst. 30 (1997) 532.
[20] H.P. Johnson, R.T. Merril, J. Geophys. Res. 77 (1972) 334.
[21] J.J. Heizmann, P. Becker, R. Baro, J. Appl. Cryst. 14 (1981) 270.
[22] R.W.G. Wyckoff, second ed., Crystal Structures, vols. 1–3, Krieger, Malabar, FL, 1982.
[23] M. Hendewerk, M. Salmeron, G.A. Somorjai, Surf. Sci. 172 (1986) 544.
[24] E. Vlieg, J. Appl. Cryst. 33 (2000) 401.
[25] F. Rohr, M. Baumer, H.-J. Freund, J.A. Mejias, V. Staemmler, S. Muller, L. Hammer, K. Heinz, Surf. Sci. 372 (1997) L291.
[26] S.J. Roosendaal, A.M. Vredenberg, F.H.P.M. Habraken, Phys. Rev. Lett. 84 (2000) 3366.
[27] O. Warschkow, D.E. Ellis, J. Hwang, N. Mansourian-Hadavi, T.O. Mason, J. Am. Ceram. Soc. 85 (2002) 213.